Chemical Engineering Science 229 (2021) 116059

Contents lists available at ScienceDirect

Chemical Engineering Science

journal homepage: www.elsevier.com/locate/ces

On the turbulence modelling of bubble plumes

Qingqing Pan [a,b,d,*], Stein Tore Johansen [a,b], Jan Erik Olsen [b], Mark Reed [c], Lars Roar Sætran [a]

[a] Department of Energy and Process Engineering, Norwegian University of Science and Technology (NTNU), Trondheim 7491, Norway
[b] Department of Process Technology, SINTEF Industry, Trondheim 7034, Norway
[c] Department of Environment and New Resources, SINTEF Ocean, Trondheim 7010, Norway
[d] National Marine Environmental Forecasting Centre (NMEFC), Ministry of Natural Resources (MNR), Beijing 100081, China

HIGHLIGHTS

- An enhanced turbulence model has been developed and validated, which is generally applicable to bubble plumes.
- The model accounts for the extra turbulence agitation introduced by bubble wakes.
- The model also considers the turbulence modulations due to bubble-induced stratification and free surface damping effects.
- The implications of each physical process in turbulence modelling are investigated.

ARTICLE INFO

Article history:
Received 23 May 2020
Received in revised form 16 August 2020
Accepted 19 August 2020
Available online 28 August 2020

Keywords:
Bubble plumes
Turbulence modelling
Free surface damping
Buoyancy-modified turbulence
Bubble-wake induced turbulence

ABSTRACT

Proper turbulence modelling of bubble plumes is critical for accurate simulation of liquid phase and bubble dynamics. The k-epsilon turbulence model is widely used. However, the model is unsatisfactory due to not accounting for the following physics: (1) turbulence damping in the vicinity of a free surface; (2) turbulence modifications created by non-uniform distribution of the bubbles; (3) extra turbulence agitation by bubble wakes. In order to remedy these deficiencies, an enhanced turbulence model has been developed, followed with application to a literature experiment of a gas-stirred ladle. The model framework is an Eulerian-Lagrangian large scale interface-capturing computational fluid dynamics (CFD) approach, coupling a volume-of-fluid model with discrete phase model. The implications of each physical process in turbulence modelling are investigated. The detailed model-experiment comparisons indicate that the enhanced turbulence model allows improved representation of the physics of bubble plumes, as well as the transport phenomena at, and close to, the free surface.

1. Introduction

Bubble plumes are common in nature and industrial applications. They can be found in systems such as reactors in chemical and environmental engineering, aeration of lakes, pneumatic oil barriers, subsea gas leakage and natural cold seeps (Cloete et al., 2009; Huda et al., 2018; Imteaz and Asaeda, 2000; McClimans et al., 2013; Sánchez et al., 2018; Xia et al., 2013; Zhang et al., 2020). Generally, there are two schools of approaches to model bubble plumes: integral plume models and multiphase computational fluid dynamics (CFD) models. Eulerian and Lagrangian integral plume models are often used as a forecasting tool, however, relying on empirical relationships and experimentally tuned parameters (Fanneløp and Sjøen, 1980; Johansen, 2000; Lee and Cheung, 1990). By contrast, multiphase CFD models can resolve the flow in a more detailed manner, by which velocities, turbulence characteristics and bubble distributions can be obtained for the whole domain. Hence, a proper CFD model is chosen as the tool for this study.

Numerical methods for computational bubble dynamics are summarized by Tomiyama (1998). In the Eulerian-Lagrangian approach, the liquid phase is solved in an Eulerian frame of reference, while the bubbles are solved in a Lagrangian frame of reference (Buwa et al., 2006; Fraga et al., 2016; Masterov et al., 2018; Olsen and Skjetne, 2020). In Eulerian-Eulerian two-fluid models, the dispersed phase and liquid phase are treated as interpenetrating continua, and each phase has its own mass and momentum conservation equations (Fleck and Rzehak, 2019; Ziegenhein et al., 2015). Herein we investigate the Lagrangian method, which has distinct advantages over the Eulerian method in terms of fewer closure requirements, ability to accommodate

* Corresponding author at: Department of Energy and Process Engineering, Norwegian University of Science and Technology (NTNU), Trondheim 7491, Norway.
E-mail address: qingqing.pan@gmail.com (Q. Pan).

https://doi.org/10.1016/j.ces.2020.116059
0009-2509/

Nomenclature

Latin

C_D	drag coefficient
E_o	Eötvös number
$\boldsymbol{F}$	total force on a single bubble (N)
$\boldsymbol{F}_{PG}$	pressure gradient force on a single bubble (N)
$\boldsymbol{F}_B$	buoyancy force on a single bubble (N)
$\boldsymbol{F}_D$	drag force on a single bubble (N)
$\boldsymbol{F}_{TD}$	turbulent dispersion force on a single bubble (N)
$\boldsymbol{F}_{VM}$	virtual mass force on a single bubble (N)
$\boldsymbol{F}_G$	gravity force on a single bubble (N)
$\boldsymbol{F}^c$	forces exerted on liquid by bubbles per unit volume (kg/m^{2}s^2),
g	gravitational constant (m/s^2)
G_B	source term in turbulent kinetic energy transport equation due to buoyancy-modified turbulence (kg/ms^3)
G_B^{ε}	source term in turbulent dissipation transport equation due to buoyancy-modified turbulence (kg/ms^4)
k	turbulent kinetic energy (m^2/s^2)
m_b	mass of a single bubble (kg)
p	pressure (N/m^2)
Re_b	bubble Reynolds number
$S_{damping}$	source term in turbulent dissipation transport equation due to free surface damping effects (kg/ms^4)
S_{wake}^k	source term in turbulent kinetic energy equation due to bubble wake effects (kg/ms^3)
S_{wake}^{ε}	source term in turbulent dissipation transport equation due to bubble wake effects (kg/ms^4)
$\boldsymbol{u}_f$	liquid velocity (m/s)
$\boldsymbol{u}_b$	Averaged bubble velocity in a computational cell (m/s)
V_{cell}	control volume (m^3)
$\boldsymbol{v}_b$	velocity of a single bubble (m/s)
$\boldsymbol{w}$	slip velocity between bubble and liquid (m/s)
x_i	coordinate direction (m)

Greek

α	volume fraction
ε	dissipation rate of turbulent kinetic energy (m^2/s^3)
κ	von Karman constant
μ	molecular viscosity (kg/ms)
μ_t	turbulent viscosity (kg/ms)
ρ	density (kg/m^3)
σ	surface tension coefficient (N/m)
τ_L	Lagrangian integral time (s)
τ_{wake}	pseudo turbulence time scale (s)
ψ	arbitrary property

Subscripts

b	bubbles
f	water phase
g	atmosphere phase (continuous gas phase)

Superscripts

ψ'	the deviation part from Reynolds decomposition

Others

$\bar{\psi}$	ensemble-averaged values

Abbreviations

CFD	computational fluid mechanics
rms	root mean square
TKE	turbulent kinetic energy

complicated exchange process, and less computational effort when further considering multiple bubble sizes (Cloete et al., 2009; Johansen and Boysan, 1988; Olsen and Skjetne, 2020, 2016). As bubble plumes in most cases end up at a free surface, the mathematical model should also be able to handle the motion and stresses at the free surface. Thus, the model framework is an Eulerian-Lagrangian large scale interface-capturing approach, coupling a discrete phase model (DPM) with a volume-of-fluid (VOF) model (Youngs, 1982) in ANSYS Fluent. The DPM is used to track bubbles in a Lagrangian frame of reference. Under the assumption of a low bubble volume fraction, the liquid phase is treated as a single phase in terms of mass conservation. However, the model accounts for the full momentum coupling between bubbles and the surrounding liquid. The VOF model solves the water and atmosphere in the Eulerian frame of reference, and captures the free surface formed by the surfacing bubble plume.

The turbulence effects in the bubble plumes are widely closed by the two-equation k-epsilon turbulence model (Besbes et al., 2015; Dhotre and Smith, 2007; Feng et al., 2020, 2015; Kataoka, 1986; Sánchez et al., 2018; Sun et al., 2020; Yum et al., 2008), due to its numerical robustness and computational efficiency. However, it has been reported by previous work that the model is unsatisfactory to simulate the plume, due to three deficiencies. First, the method underpredicts surface velocities due to incomplete turbulence modelling near the free surface. Second, the model does not account for turbulence modifications due to the density stratification created by vertical non-uniform distribution of bubbles. And third, the model also neglects the extra turbulence agitation introduced by bubbles into the liquid through wake effects, which affect plume spreading (Cloete et al., 2009; Johansen and Boysan, 1988; Olsen and Skjetne, 2016; Wu et al., 2017). There is little work in the literature on the extension of a two-equation model to resolve the above three missing physical processes. The implications of each process in turbulence modelling are also interesting to investigate.

Thus, this study aims to develop an enhanced k-epsilon turbulence model to make it more generally applicable to bubble plumes. The enhanced model is applied to the gas-stirred ladle experiment carried out by Johansen et al. (1988) and Elgsæter (1986). The model framework is an Eulerian-Lagrangian-large scale interface-capturing approach combing DPM and VOF. The detailed comparison with experimental data, in terms of mean flow, turbulence and bubble distribution, indicate that the enhanced turbulence model allows improved representation of the physics of bubble plumes, as well as the transport phenomena at, and close to, the free surface.

2. Model framework

2.1. Bubble dynamics

Bubbles are tracked by solving the force balance equation due to Newton's second law, where the acceleration equates the forces acting on the bubbles. Note that the motion of the bubbles is also affected by chemical reactions and mass transfer, and these processes are not considered here.

$$\frac{d\boldsymbol{v}_b}{dt}=\frac{\boldsymbol{F}}{m_b}=\frac{\boldsymbol{F}_D+\boldsymbol{F}_{TD}+\boldsymbol{F}_B+\boldsymbol{F}_G+\boldsymbol{F}_{VM}+\boldsymbol{F}_{PG}}{m_b}$$
$$=\frac{18\mu}{\rho_b d_b^2}\frac{C_D Re_b}{24}(\boldsymbol{u}_f-\boldsymbol{v}_b)+\frac{\rho_b-\rho_f}{\rho_b}\boldsymbol{g}+C_v\frac{\rho_f}{\rho_b}\left(\frac{D\boldsymbol{u}_f}{Dt}-\frac{d\boldsymbol{v}_b}{dt}\right)+\frac{\rho_f}{\rho_b}\frac{D\boldsymbol{u}_f}{Dt} \tag{1}$$

where, $\boldsymbol{v}_b$, m_b, ρ_b and d_b are the velocity, mass, density and diameter of the bubbles. μ, $\boldsymbol{u}_f$ and ρ_f are the molecular viscosity, instantaneous velocity and density of the liquid. C_D is bubble drag coefficient expressed below. Re_b is bubble Reynolds number, defined as $Re_b=\rho_f d_b|\boldsymbol{u}_f-\boldsymbol{v}_b|/\mu$. The forces are bubble drag force $\boldsymbol{F}_D$, turbulent dispersion force $\boldsymbol{F}_{TD}$, buoyancy force $\boldsymbol{F}_B$, gravity force $\boldsymbol{F}_G$, virtual mass force $\boldsymbol{F}_{VM}$ and pressure gradient force $\boldsymbol{F}_{PG}$ per bubble mass respectively. Note that bubble–bubble interactions are not considered.

The instantaneous velocity $\boldsymbol{u}_f$ is subdivided into the Reynolds-averaged velocity $\bar{\boldsymbol{u}}_f$ and velocity fluctuations $\boldsymbol{u}_f'$. The slip velocity in the drag formulation is in most implementations based on the mean velocity $\bar{\boldsymbol{u}}_f$. The remaining stress on the bubbles due to fluctuation is expressed in the turbulent dispersion force $\boldsymbol{F}_{TD}=\frac{18\mu}{\rho_b d_b^2}\frac{C_D Re_b}{24}\boldsymbol{u}_f'$. It is random in nature and causes spreading of the turbulent plume. $\boldsymbol{u}_f'$ are extracted by a normally distributed random number ζ and the standard deviation $\sqrt{2/3k}$, i.e.$u_i'=\zeta\sqrt{2/3k}$, where k is turbulent kinetic energy (TKE). Turbulent dispersion of the bubbles was implemented using a stochastic tracking approach, governed by the smaller one of the eddy lifetime and time spent by a bubble inside the turbulent eddy (Gosman and Loannides, 1983).

Here we take the virtual mass coefficient C_v = 0.5, which is the analytical value for a sphere. Lift force was assumed insignificant for relatively high flowrates (Olsen and Popescu, 2012). The Basset force is not considered here due to the complexity, also it is a low Reynolds number force that has no application where bubble Reynolds numbers are significantly larger than 1.0 (Johansen, 1990).

A widely recognized bubble drag law was published by Tomiyama (1998). The drag coefficients depend on bubble Reynolds number Re_b, Eötvös number Eo and degree of contamination of the water in which the bubble is rising. Here we take the bubble drag coefficient in a slightly contaminated water (Tomiyama, 1998):

$$C_D=\max\left\{\min\left[\frac{24}{Re_b}\left(1+0.15Re_b^{0.687}\right),\frac{72}{Re_b}\right],\frac{8}{3}\frac{Eo}{Eo+4}\right\} \tag{2}$$

where, $Eo=g\left(\rho_f-\rho_b\right)d_b^2/\sigma$, σ is the surface tension coefficient.

Eq. (1) is solved supplemented by the following kinematic relationship which defines the trajectory of the bubble:

$$\frac{d\boldsymbol{x}_b}{dt}=\boldsymbol{v}_b \tag{3}$$

where, $\boldsymbol{x}_b$ is the position of the bubble.

Due to Newton's third law, the coupling forces exerted on the liquid by bubbles are the same in magnitude but opposite in direction of the forces acting on bubbles from the liquid. By collecting the drag and virtual mass force on all the bubbles in a computational cell, the coupling force $\boldsymbol{F}^c$ to the liquid per unit volume can be obtained as:

$$\boldsymbol{F}^c=-\frac{1}{V_{cell}}\sum_{m=1}^{N}\left(\boldsymbol{F}_{D,m}+\boldsymbol{F}_{\mathrm{VM,m}}\right) \tag{4}$$

where, V_{cell} is the volume of the computational cell, N is the total count of bubbles in the cell.

2.2. Free surface flow

The VOF method employs an advanced interface tracking scheme known as Youngs' VOF (Youngs, 1982) to track the interface through the Eulerian mesh. If a cell is found to consist of two or more phases, an interface must be interpolated through it. The volume fraction conservation equations for water (f) and atmosphere (g) are solved. Note that liquid displacement by bubbles is neglected.

$$\frac{\partial}{\partial t}\alpha_k+\bar{u}_j\cdot\frac{\partial\alpha_k}{\partial x_j}=0 \tag{5}$$

with constant density $\rho_{k=f,g}$ and constraints $\alpha_g+\alpha_f=1$.

where, α_k is the volume fraction of phase $k=f,g$.

Momentum conservation is given by a single set of Reynolds-averaged Navier-Stokes equations.

$$\frac{\partial}{\partial t}\left(\rho\bar{u}_i\right)+\frac{\partial}{\partial x_j}(\rho\bar{u}_i\bar{u}_j)=-\frac{\partial\bar{p}}{\partial x_i}+\frac{\partial}{\partial x_j}\left[\mu\left(\frac{\partial\bar{u}_i}{\partial x_j}+\frac{\partial\bar{u}_j}{\partial x_i}\right)\right]-\frac{\partial}{\partial x_j}\left(\rho\,\overline{u_i'u_j'}\right)$$
$$+\rho g_i+\bar{F}_i^c+\sigma\frac{\rho H_g\frac{\partial\alpha_g}{\partial x_i}}{\frac{1}{2}\left(\rho_g+\rho_f\right)} \tag{6}$$

where, density and molecular viscosity are volume-averaged properties $\rho=\sum\alpha_k\rho_k$ and $\mu=\sum\alpha_k\mu_k$. p is the pressure. The last term on the right hand side is the surface tension force, where the interface curvature is $H=\nabla\cdot\left(\frac{\nabla\alpha_k}{|\nabla\alpha_k|}\right)$, with $H_g=-H_f$ and $\nabla\alpha_g=-\nabla\alpha_f$. For the coupling force F_i^c, refer to Eq. (4).

Through the Boussinesq hypothesis, the turbulent stress is represented by:

$$\rho\,\overline{u_i'u_j'}=\frac{2}{3}\rho k\delta_{ij}-\mu_t\left(\frac{\partial\bar{u}_i}{\partial x_j}+\frac{\partial\bar{u}_j}{\partial x_i}\right) \tag{7}$$

where, μ_t is turbulent viscosity.

The system can be closed by the following standard k-epsilon model.

The TKE transport equation reads:

$$\rho\frac{\partial k}{\partial t}+\rho\bar{u}_j\frac{\partial k}{\partial x_j}=\mu_t\left(\frac{\partial\bar{u}_i}{\partial x_j}+\frac{\partial\bar{u}_j}{\partial x_i}\right)\frac{\partial\bar{u}_i}{\partial x_j}+\frac{\partial}{\partial x_j}\left[\left(\mu+\frac{\mu_t}{\sigma_k}\right)\frac{\partial k}{\partial x_j}\right]-\rho\varepsilon \tag{8}$$

The turbulent dissipation transport equation reads:

$$\rho\frac{\partial\varepsilon}{\partial t}+\rho\bar{u}_j\frac{\partial\varepsilon}{\partial x_j}=C_{1\varepsilon}\frac{\varepsilon}{k}\left[\mu_t\left(\frac{\partial\bar{u}_i}{\partial x_j}+\frac{\partial\bar{u}_j}{\partial x_i}\right)\frac{\partial\bar{u}_i}{\partial x_j}\right]$$
$$+\frac{\partial}{\partial x_j}\left[\left(\mu+\frac{\mu_t}{\sigma_\varepsilon}\right)\frac{\partial\varepsilon}{\partial x_j}\right]-\rho C_{2\varepsilon}\frac{\varepsilon^2}{k} \tag{9}$$

where, ε is turbulent dissipation. $C_\mu,\sigma_k,\sigma_\varepsilon,C_{1\varepsilon},C_{2\varepsilon}$ are given values of 0.09, 1.0, 1.3, 1.44 and 1.92, respectively, as Launder and Spalding (1983).

3. Turbulence modelling

To make the turbulence model more generally applicable to bubble plumes, the standard k-epsilon model is extended to account for the following physics: (1) turbulence damping in the vicinity of a free surface; (2) turbulence modifications due to the density variation created by the non-uniform distribution of the bubbles; (3) extra turbulence agitation introduced by bubbles into the liquid through wakes. These are modelled as source terms in the transport equation of TKE and its dissipation.

3.1. Free surface damping

The standard k-epsilon model underpredicts the surface velocity and overpredicts the TKE at the free surface, compared to experiments. This is due to a phenomenon of increased turbulence kinetic energy dissipation in the proximity of the free surface, which is not captured by the standard model. When turbulent eddies approach and locally lift a free surface, the turbulence is damped by the stagnation pressure (Cloete et al., 2009; Olsen and Skjetne, 2016; Sheng and Irons, 1993; Soga and Rehmann, 2004).

According to the interface-modulated turbulence model proposed by Naot and Rodi (1983), here we extend the standard k-epsilon model to account for the presence of the free surface. Being aware that the epsilon transport equation is actually the eddy length scale equation, a model is required to supply the correct characteristic length to treat the near surface turbulence, and this model should assure the length scale is zero at the free surface. Then a proportional relationship between the eddy length scale l_0 and the physical distance to the free surface l_s is proposed in Eq. (10). The modelled epsilon ε_{new} is designed to override the epsilon value in computational cells near the surface through a source term $S_{damping}$, shown by Eq. (11) (Olsen and Skjetne, 2016; Pan et al., 2013). This source term is added in the turbulent dissipation transport equation, shown in Eq. (25) in Section 3.4.

$$l_0 = \kappa l_s, l_0 \approx \left(\frac{\upsilon_t^3}{\varepsilon_{new}}\right)^{1/4} = \frac{C_\mu^{3/4} k^{3/2}}{\varepsilon_{new}}, \varepsilon_{new} = \frac{C_\mu^{3/4} k^{3/2}}{\kappa l_s} \tag{10}$$

$$S_{damping} = \frac{\text{large\_number} \cdot \rho(\varepsilon_{new} - \varepsilon)}{\Delta t} \tag{11}$$

where, κ=0.4 is the von Karman constant. ρ is the volume-averaged density defined previously.Δt is the fluid time step, which is on the denominator to be consistent with the unit of the turbulent dissipation rate. One should be careful with the choice of 'large_number' in Eq. (11), it should be sufficiently large to force the transport equation to approach ε_{new} and at the same time avoid stability issues. Different scenarios of 10, 100, 1000, 10,000 were tested and 1000 satisfied the requirements.

3.2. Buoyancy-modified turbulence

Due to the non-uniform distribution of bubbles, there is added turbulence intensity in unstable stratified flow regions and suppressed turbulence in stable stratified flows. Since the standard k-epsilon model was developed for constant density flows, a source term has to be added to account for the effects of buoyancy.

The momentum transport equations for liquid phase and bubble phase in the Eulerian frame of reference are as follows according to Ishii (1975):

$$\frac{\partial}{\partial t}\left(\rho_f \alpha_f u_{fi}\right) + \frac{\partial}{\partial x_j}\left(\rho_f \alpha_f u_{fi} u_{fj}\right) = -\alpha_f \frac{\partial p}{\partial x_j} + \frac{\partial}{\partial x_j}\left(\alpha_f \mu_f \left(\frac{\partial u_{fi}}{\partial x_j} + \frac{\partial u_{fj}}{\partial x_i}\right)\right) + F_i^c + \alpha_f \rho_f g_i \tag{12}$$

$$\frac{\partial}{\partial t}\left(\rho_b \alpha_b u_{bi}\right) + \frac{\partial}{\partial x_j}\left(\rho_b \alpha_b u_{bi} u_{bj}\right) = -\alpha_b \frac{\partial p}{\partial x_j} + \frac{\partial}{\partial x_j}\left(\alpha_b \mu_b \left(\frac{\partial u_{bi}}{\partial x_j} + \frac{\partial u_{bj}}{\partial x_i}\right)\right) - F_i^c + \alpha_b \rho_b g_i \tag{13}$$

where, $\boldsymbol{u}_b$ is bubble velocity in a cell defined as $\boldsymbol{u}_b = \sum_{m=1}^{N} \boldsymbol{v}_{b,m}/N$. Since the internal flow in the bubbles can be neglected, the viscous stress term in Eq. (13) can be neglected.

By adding (12) and (13), the mixture model is obtained, which describes the momentum transport of the mixture of water and gas bubbles:

$$\begin{aligned} &\frac{\partial}{\partial t}\left(\rho_f \alpha_f u_{fi} + \rho_b \alpha_b u_{bi}\right) + \frac{\partial}{\partial x_j}\left(\rho_f \alpha_f u_{fi} u_{fj} + \rho_b \alpha_b u_{bi} u_{bj}\right) \\ &= -\frac{\partial p}{\partial x_j} + \frac{\partial}{\partial x_j}\left(\alpha_f \mu_f \left(\frac{\partial u_{fi}}{\partial x_j} + \frac{\partial u_{fj}}{\partial x_i}\right)\right) + \left(\alpha_f \rho_f + \alpha_b \rho_b\right) g_i \\ &= \underbrace{-\frac{\partial p}{\partial x_j} + \frac{\partial}{\partial x_j}\left(\alpha_f \mu_f \left(\frac{\partial u_{fi}}{\partial x_j} + \frac{\partial u_{fj}}{\partial x_i}\right)\right) + \rho_f g_i}_{\text{single - phase like term}} \underbrace{-\alpha_b \left(\rho_f - \rho_b\right) g_i}_{\text{due to bubbles}} \end{aligned} \tag{14}$$

The right hand side of (14) can be divided into two parts. One part is single-phase like terms; the other part arises from the presence of bubbles.

From the mixture point of view in Eq. (14), it is seen that the plume is driven by the buoyancy force $-\alpha_b\left(\rho_f - \rho_b\right) g_i$. The density variations would result in gradients of bubble volume fraction in space. Now we explore the contribution of buoyancy force to the production and destruction of turbulence. The variation in the buoyancy force $f_i = -\alpha_b\left(\rho_f - \rho_b\right) g_i$ around its ensemble-averaged value is expressed as:

$$f_i' = -\alpha_b'\left(\rho_f - \rho_b\right) g_i \tag{15}$$

where, f_i is the buoyancy force of the bubbles, α_b is bubble volume fraction.

The contribution to turbulence modification is obtained by multiplying u_i' to Eq. (15), and then performing ensemble averaging, using the same technique as in the derivation of the TKE equation. Through the first order Taylor expansion with respect to the mixing length l_m, the variations of volume fraction α_b' are connected to the ensemble-averaged values $\bar{\alpha}_b$. Reynolds stresses arise from the relationship $l_m = u_m' \cdot \tau_L$(Johansen, 1990), where u_m' is the fluctuating velocity part in the ensemble averaging operation. The Lagrangian integral time is estimated as $\tau_L = 0.15k/\varepsilon$, according to Daly and Harlow (1970).

Turbulent production due to buoyancy then becomes:

$$\begin{aligned} G_B &= \overline{f_i' u_i'} = -\left(\rho_f - \rho_b\right) \cdot \overline{\alpha_b' u_i'} \cdot g_i \\ &= \left(\rho_f - \rho_b\right) l_m \frac{\partial \bar{\alpha}_b}{\partial x_m} \overline{u_i'} \cdot g_i \\ &= \left(\rho_f - \rho_b\right) \left(u_m' \cdot \tau_L\right) \cdot \overline{u_i'} \cdot \frac{\partial \bar{\alpha}_b}{\partial x_m} \cdot g_i \\ &= \left(\rho_f - \rho_b\right) \overline{u_1' u_3'} \cdot \tau_L \cdot \frac{\partial \bar{\alpha}_b}{\partial x} \cdot g_z + \left(\rho_f - \rho_b\right) \overline{u_2' u_3'} \cdot \tau_L \cdot \frac{\partial \bar{\alpha}_b}{\partial y} \cdot g_z + \left(\rho_f - \rho_b\right) \overline{u_3' u_3'} \cdot \tau_L \cdot \frac{\partial \bar{\alpha}_b}{\partial z} \cdot g_z \\ &= -\frac{\rho_f - \rho_b}{\rho_f} \mu_t \left(\frac{\partial \bar{u}_1}{\partial z} + \frac{\partial \bar{u}_3}{\partial x}\right) \cdot \tau_L \cdot \frac{\partial \bar{\alpha}_b}{\partial x} \cdot g_z - \frac{\rho_f - \rho_b}{\rho_f} \mu_t \left(\frac{\partial \bar{u}_2}{\partial z} + \frac{\partial \bar{u}_3}{\partial y}\right) \cdot \tau_L \cdot \frac{\partial \bar{\alpha}_b}{\partial y} \cdot g_z \\ &\quad + \left(\rho_f - \rho_b\right) \cdot \frac{2}{3} k \cdot \tau_L \cdot \frac{\partial \bar{\alpha}_b}{\partial z} \cdot g_z \end{aligned} \tag{16}$$

where,u_1, u_2 and u_3 are velocity components in x, y and z directions. Note that this source term is for water phase only.

The corresponding source term in the turbulent dissipation transport equation G_B^ε is obtained through dividing the above TKE source term by a time scale k/ε. The degree to turbulent dissipation affected by the buoyancy is determined by a constant C_{ε_buo}, and calculated using the following relation (Henkes et al., 1991):

$$G_B^\varepsilon = \frac{C_{\varepsilon\_buo} \cdot G_B}{k/\varepsilon} = 1.44 \cdot \tanh\left(\left|\frac{\bar{u}_3}{\sqrt{\bar{u}_1^2 + \bar{u}_2^2}}\right|\right) \cdot \frac{\varepsilon}{\kappa} \cdot G_B \tag{17}$$

3.3. Bubble-wake induced turbulence

Lance and Bataille (1991) have made the observation that bubbles can contribute to extra agitation in the flow. Earlier researchers have treated the pseudo turbulence to be linearly superimposed on the normal shear-induced turbulence. Sato and

Sekoguchi (1975) accounted for bubble-induced turbulence by an extra turbulent viscosity. Van Wijngaarden (1998) and Lopez de Bertodano et al. (1994) modelled the drag-induced turbulence as an extra pseudo TKE, which was added to the normal TKE to have the total TKE. Researchers more frequently modelled the bubble agitated turbulence as the source terms in the turbulence transport equations (Feng et al., 2015; Rzehak and Krepper, 2013; Troshko and Hassan, 2001). Vaidheeswaran and Hibiki (2017) have reviewed different modelling strategies for bubble induced turbulence, and there is still a lack of universal approach which could be attributed to the inherent range of spatio-temporal scales in two-phase bubbly flows. Risso (2018) pointed out that the mechanism driving the turbulence production by bubble agitation still needs to be elucidated.

Pan (2014) has derived, using combined Favre and volume averaging on the governing equations, that the shear work performed on the liquid by bubbles is equal to the product of the drag force on the liquid and the relative velocity, that is $S^k_{wake} = \boldsymbol{F}^c_D \cdot (\boldsymbol{u}_b - \boldsymbol{u}_f)$, which can be interpreted as the additional turbulence production due to bubble wakes. The drag force exerted on the liquid per unit volume from bubbles is arranged as:

$$\begin{aligned}\bar{\boldsymbol{F}}^c_D &= -\frac{1}{V_{cell}}\sum_{m=1}^{N}\boldsymbol{F}_{D,m} \approx -N\cdot\boldsymbol{F}_D = -\frac{\alpha_b}{V_b}\cdot\boldsymbol{F}_D = -\frac{\alpha_b}{\frac{\pi}{6}d_b^3}\frac{1}{2}C_D\rho_f\frac{\pi}{4}d_b^2\left|\bar{\boldsymbol{u}}_f-\bar{\boldsymbol{u}}_b\right|\left(\bar{\boldsymbol{u}}_f-\bar{\boldsymbol{u}}_b\right)\\ &\approx -\frac{3}{4d_b}\alpha_b C_D\rho_f\left|\bar{\boldsymbol{u}}_f-\bar{\boldsymbol{u}}_b\right|\left(\bar{\boldsymbol{u}}_f-\bar{\boldsymbol{u}}_b\right)\end{aligned} \tag{18}$$

then, the source term S^k_{wake} to the TKE equation in the ensemble-averaging framework can be obtained as follows:

$$\begin{aligned}S^k_{wake} = \bar{\boldsymbol{F}}^c_D\left(\bar{\boldsymbol{u}}_b-\bar{\boldsymbol{u}}_f\right) &= -\tfrac{3}{4d_b}\alpha_b C_D\rho_f\left|\bar{\boldsymbol{u}}_f-\bar{\boldsymbol{u}}_b\right|\left(\bar{\boldsymbol{u}}_f-\bar{\boldsymbol{u}}_b\right)\left(\bar{\boldsymbol{u}}_b-\bar{\boldsymbol{u}}_f\right)\\ &= \tfrac{3}{4}\alpha_b\rho_f\tfrac{C_D}{d_b}\left|\bar{\boldsymbol{u}}_b-\bar{\boldsymbol{u}}_f\right|^3\end{aligned} \tag{19}$$

Analogous to the buoyancy-modified turbulence model, the corresponding source term in turbulent dissipation transport equation can be obtained through dividing the TKE source term by an appropriate time scale. This time scale has been modelled based on dimensional analysis. We estimate that the mixing length scale of the bubble wake l_{wake} should be comparable to the bubble size d_b as proposed in Eq. (20). By introducing the pseudo turbulence intensity $0 < \delta < 1$, the rms pseudo turbulent velocity $\sqrt{\bar{u'^2_{wake}}}$ is proportionally connected to the ensemble-averaged slip velocity magnitude as seen in Eq. (21). From the length and velocity scale, we can obtain the pseudo turbulence time scale τ_{wake}, as Eq. (22).

$$l_{wake} = \kappa d_b \tag{20}$$

$$\sqrt{\bar{u'^2_{wake}}} = \sqrt{\frac{2}{3}k_{wake}} = \delta\cdot|\bar{\boldsymbol{w}}| \tag{21}$$

$$\tau_{wake} = \frac{l_{wake}}{\sqrt{\bar{u'^2_{wake}}}} = \frac{\kappa d_b}{\delta\cdot|\bar{\boldsymbol{w}}|} \tag{22}$$

With the source term to the TKE equation expressed in Eq. (19), the corresponding source term in the turbulent dissipation transport equation S^ε_{wake} can thus be modelled using the time scale τ_{wake} and a coefficient C^ε_{wake}.

$$S^\varepsilon_{wake} = \frac{C^\varepsilon_{wake}\cdot S^k_{wake}}{\tau_{wake}} = \frac{C^\varepsilon_{wake}\cdot\delta\cdot\left|\bar{\boldsymbol{w}}\right|\cdot S^k_{wake}}{\kappa d_b} \tag{23}$$

3.4. The enhanced turbulence model

Summing up Sections 3.1–3.3, we conclude with the complete version of the enhanced turbulence model:

$$\rho\frac{\partial k}{\partial t}+\rho\bar{u}_j\frac{\partial k}{\partial x_j} = \mu_t\left(\frac{\partial\bar{u}_i}{\partial x_j}+\frac{\partial\bar{u}_j}{\partial x_i}\right)\frac{\partial\bar{u}_i}{\partial x_j}+\frac{\partial}{\partial x_j}\left[\left(\mu+\frac{\mu_t}{\sigma_k}\right)\frac{\partial k}{\partial x_j}\right] - \rho\varepsilon+\underbrace{G_B+S^k_{wake}}_{\text{source term}} \tag{24}$$

$$\rho\tfrac{\partial\varepsilon}{\partial t}+\rho\bar{u}_j\tfrac{\partial\varepsilon}{\partial x_j} = C_{1\varepsilon}\tfrac{\varepsilon}{k}\left[\mu_t\left(\tfrac{\partial\bar{u}_i}{\partial x_j}+\tfrac{\partial\bar{u}_j}{\partial x_i}\right)\tfrac{\partial\bar{u}_i}{\partial x_j}\right]+\tfrac{\partial}{\partial x_j}\left[\left(\mu+\tfrac{\mu_t}{\sigma_\varepsilon}\right)\tfrac{\partial\varepsilon}{\partial x_j}\right]-\rho C_{2\varepsilon}\tfrac{\varepsilon^2}{k} +\underbrace{S_{damping}+G^\varepsilon_B+S^\varepsilon_{wake}}_{\text{source term}} \tag{25}$$

Eqs. (16), (19), (11), (17), (23). The source terms in Eqs. (24) and (25) have been implemented in ANSYS Fluent 19.0 with a set of user defined functions.

In order to investigate the influence of each process to the plume dynamics, the source terms are also implemented separately as follows: $S_{damping}$ for free surface damping module, G_B and G^ε_B for buoyancy-modified turbulence module, S^k_{wake} and S^ε_{wake} for bubble-wake induced turbulence module.

4. Results and discussions

The standard and enhanced k-epsilon turbulence model has been applied to the experiment of Johansen et al. (1988) and Elgsæter (1986). To set up a simulation, the choice of grid and time steps are firstly studied by dependency studies, followed with the analysis of the integral property. The enhanced turbulence modelling accounting for each process, that is the free surface damping, non-uniform distribution of bubbles and bubble wake, were then investigated separately. The improvement of the complete version of the enhanced model with respect to the standard model was evaluated. The significance of the parameter in the bubble-wake induced turbulence model was discussed. And the validation study of the proposed turbulence model against the experimental observations was carried out last.

The modelling concept and simulated ladle geometry for the experiment is shown schematically in Fig. 1. The ladle is of conical-cylinder shape with initial free surface height of 1.237 m, and with top and bottom diameters of 1.1 m and 0.93 m. The computational domain height is extended to 1.5 m to involve the atmosphere above. In the experiment, gas is injected through a centrally located 5 cm diameter porous plug with different flowrates: 1.3×10^{-4} m^3/s, 2.7×10^{-4} m^3/s, 4.7×10^{-4} m^3/s and 6.1×10^{-4} m^3/s at atmospheric pressure. The data set with 4.7×10^{-4} m^3/s was used to develop the enhanced turbulence model and simulation setup (Section 4.1–4.4), while the other data sets were used to validate the proposed turbulence model (Section 4.5). The averaged bubble diameter is assumed to be 2 mm for the two lower flowrates and 3 mm for the two higher flowrates, according to $d_b \approx 25\%\times0.35\times\left(Q^2/g\right)^{0.2}$ as Johansen and Boysan (1988). The bubbles are removed upon entering the gas phase. In the experiment, observations were obtained near the bottom (0.113 m height), half-way up (0.625 m height), and near the free surface (1.027 m, 1.117 m, and 1.222 m heights), as seen in Fig. 1.

4.1. Dependency studies

A series of sensitivity studies on mesh size, flow time step, number of computational parcels, as well as steady state, are performed

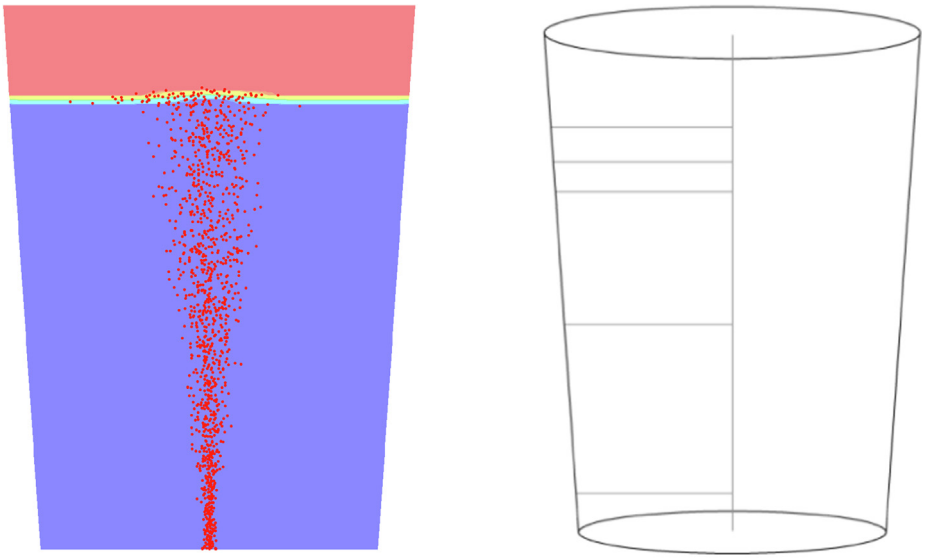

Fig. 1. (a) A snapshot of the Lagrangian bubbles and the interface between the water and the atmosphere; (b) schematic of the 3D physical domain of the gas-stirred-ladle experiment, in which the observations were obtained from 5 heights. (For interpretation of the references to colour in this figure legend, the reader is referred to the web version of this article.)

to seek the most appropriate simulation parameters. The standard k-epsilon model was run with flowrate of 4.7×10^{-4} m^3/s in these studies.

The grid resolution employed here is arrived at by a grid independence study. The grids have been refined at the free surface region. To seek a proper grid system, five different grid systems of (plume, free surface) = (5 cm, 3 cm), (4 cm, 2 cm), (3 cm, 1.5 cm), (2 cm, 1.5 cm) and (1 cm, 1 cm) were tested. Fig. 2a displays the distribution of axial mean velocity at 0.625 m height. It can be seen that the velocity profiles on the grids of (2 cm, 1.5 cm) and (1 cm, 1 cm) coincide, which implies that the resolution of 2 cm cell in the plume region and 1.5 cm cell at the free surface region can satisfy the requirement of grid independence. The following simulations were performed on this grid, which is 141 960 hexahedral cells as seen in Fig. 2b-c. Three flow time steps, 0.03 s, 0.01 s and 0.003 s, which comply with the CFL criterion, were also tested. No difference in simulating the plume are observed upon switching a time step 0.01 s to a smaller value of 0.003 s. Thus, 0.01 s is chosen for the flow time step in the following simulations.

Discrete bubble parcels, the computational parcels, contain a group of bubbles with the same characteristics. The mass of a parcel is equal to the product of total mass flowrate and the injection time step, and then dividing by the number of streams which is set to be 10 in all the simulations. The parcel mass and the resulting number of parcels are thus governed by this injection time step, which can be different from the flow time step. The parcel number tracked involves a trade-off between the computational efforts and proper representation of the plume. Three injection time steps, 0.01 s, 0.003 s and 0.001 s, were tested, which correspond to ~2000, 6000–7000, ~20000 parcels in order of magnitude. The distribution of liquid velocity and bubble volume fraction are consistent when comparing the 0.003 s and 0.001 s cases. In the following simulations, bubble parcels are thus set to be released from each stream every 0.003 s.

The transient simulation was run until no significant change could be observed in the monitored liquid velocity and bubble volume fraction. As seen in Fig. 3, there is negligible variation in the axial mean velocity at the plume centre of 0.625 m height, after a steady state is reached. Thus, no time averaging is necessary for the liquid velocities. This is also because the inherent Reynolds-averaged Navier-Stokes nature of the approach provided an averaged representation of the plume. The possible plume wandering is not observed in the simulation, which is consistent with the experiment. However, there are slight fluctuations in the bubble volume fraction with time. Thus, the bubble statistics would require further time averaging. It is also confirmed that circumferential averages with respect to radial coordinates match the results sampled in any single angular direction, so the simulation results are given at 0 degrees.

4.2. Integral property

The integral property is investigated, in order to ensure the proper implementation of the turbulence models. Driven by the same air flowrate 4.7×10^{-4} m^3/s, the calculated velocity vectors and bubble distributions closed by the standard and the complete version of the enhanced turbulence model are shown in Fig. 4. Compared with the standard model, the enhance model produced a plume with slower upwelling and more dispersion. The eye of toroidal recirculation zone located more toward the cylindrical wall in the upper half of the ladle. Both simulations are run with the same air volume flux 4.7×10^{-4} m^3/s at standard conditions. Due to slight compression by pressure, the air volume flux is 4.4×10^{-4} m^3/s at height of 0.625 m. The total air volume flux is obtained by integrating the product of the local bubble velocity and bubble volume fraction, according to Milgram (1983), that is $q = 2\pi \int_0^\infty \left(\left|\bar{\boldsymbol{u}}_b\right| \cdot \alpha_b\right) r dr$, where q is the total air volume flux, $\left|\bar{\boldsymbol{u}}_b\right|$ is bubble velocity magnitude, α_b is bubble volume fraction, and r is the radial coordinate. The comparisons of the distribution of bubble velocity magnitude and bubble volume fraction at half way up is shown in Fig. 5. By the integration operations for the standard and enhanced model implementations, the total volume flux is 4.5×10^{-4} m^3/s and 4.6×10^{-4} m^3/s, respectively, with the deviation from the theoretical value 4.4×10^{-4} m^3/s being 1.3% and 2.7%. Thus, it can be concluded that the integral property is properly conserved.

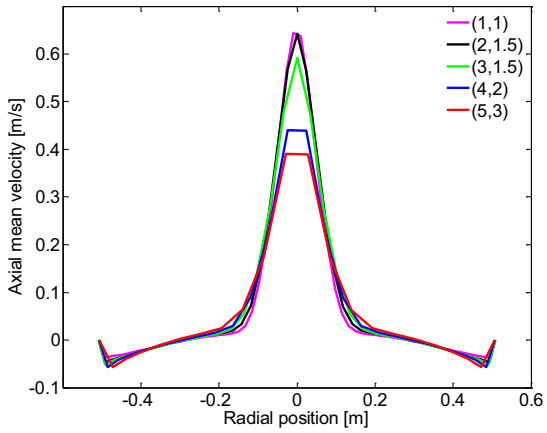

(a)

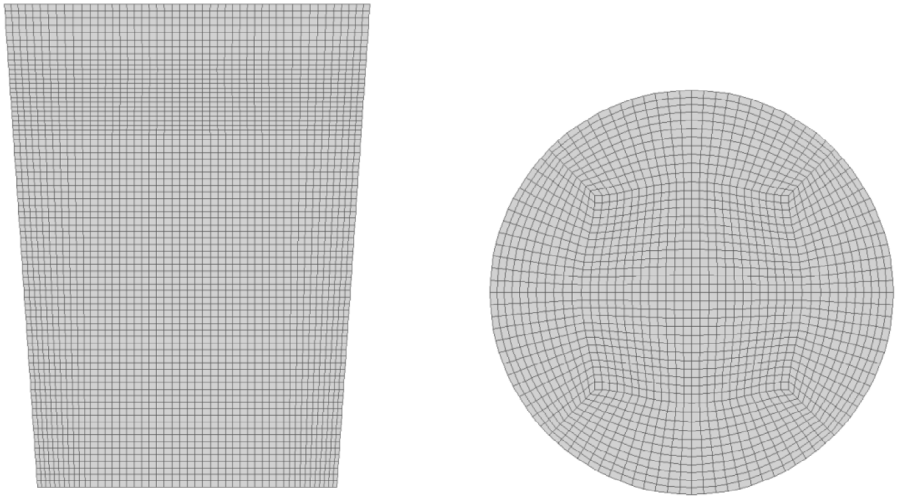

(b) (c)

Fig. 2. (a) Simulated profiles of axial mean velocity along radial position at 0.625 m height on five different grid systems of (plume, free surface) = (5 cm, 3 cm), (4 cm, 2 cm), (3 cm, 1.5 cm), (2 cm, 1.5 cm) and (1 cm, 1 cm) with flowrate of 4.7×10^{-4} m^3/s; (b) the chosen grid in the axial centre plane; (c) the chosen grid at the interface.

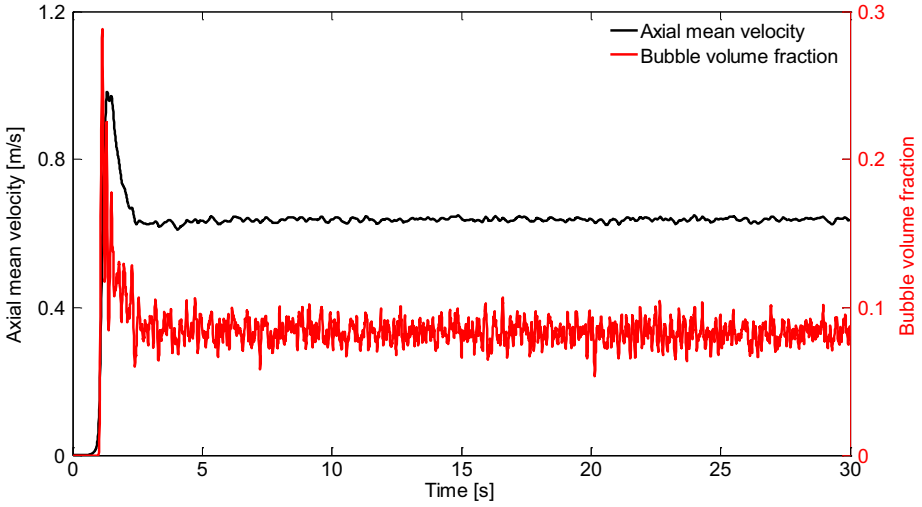

Fig. 3. Time series of simulated axial mean velocity and bubble volume fraction at the plume centre of 0.625 m height with flowrate of 4.7×10^{-4} m^3/s.

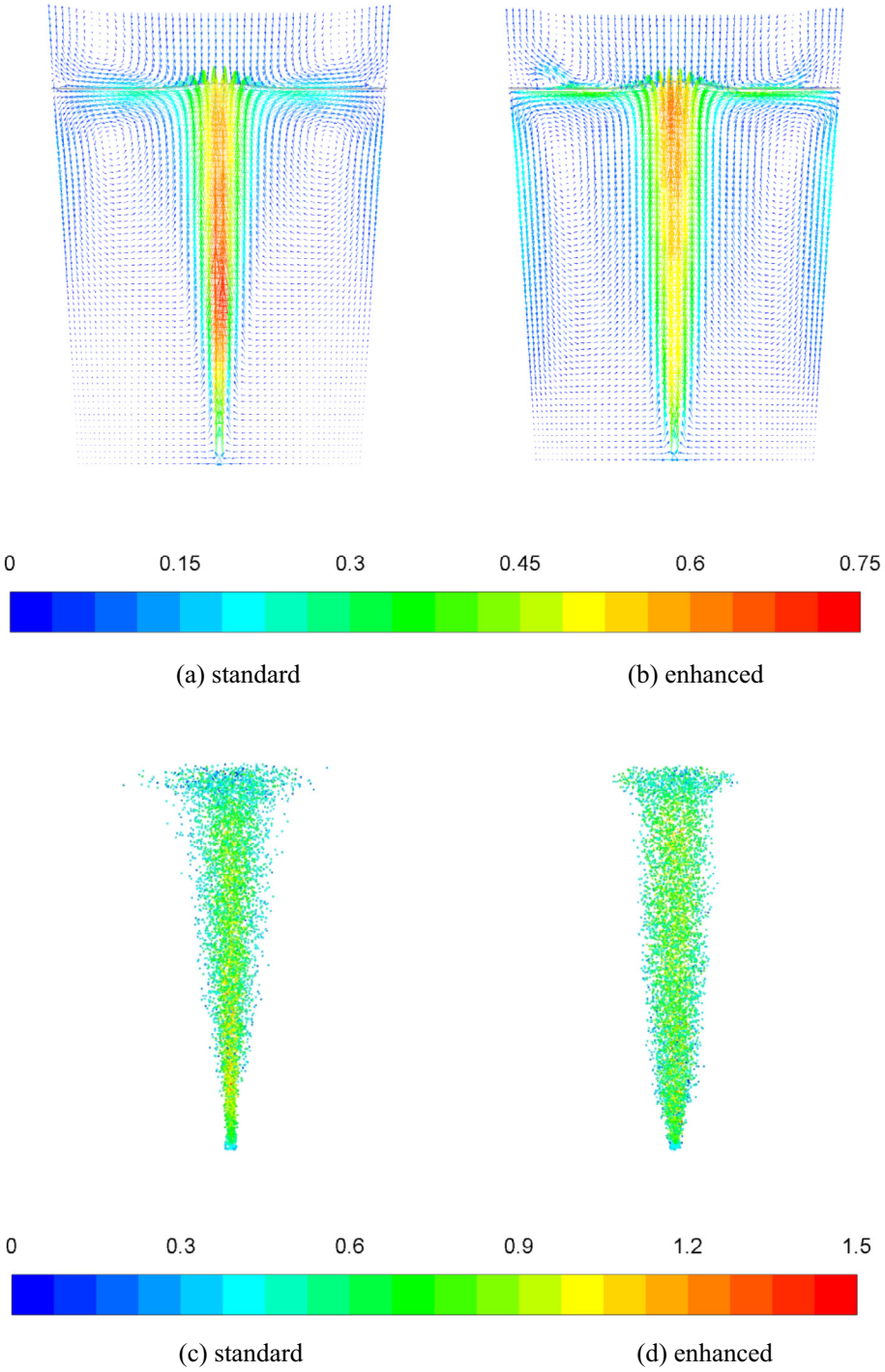

Fig. 4. Simulated velocity vector coloured by velocity magnitude (a,b) and bubble cloud coloured by bubble velocity magnitude (c,d) in the standard and enhanced turbulence model implementations, respectively, with flowrate of 4.7×10^{-4} m^3/s. The location of the free surface is indicated by grey curves.

4.3. Enhanced turbulence modelling

In order to investigate the influence of the enhanced turbulence modelling to the plume with respect to the standard model, the following model runs were carried out: each module, that is, free surface damping ('damping'), buoyancy-modified turbulence ('buoyancy') and bubble-wake induced turbulence ('wake') was implemented separately, together with a complete version of the enhanced model ('enhanced') including the above three modules. A detailed comparison between the simulation results and the experimental data for flowrate of 4.7×10^{-4} m^3/s are shown in Figs. 6–9, in terms of radial mean velocity components $\bar{u}_r$, axial mean velocity components $\bar{u}_z$, turbulent velocities $\sqrt{2/3k}$ and bubble volume fraction α_b.

It is demonstrated the standard model (red solid lines) underestimated both the radial and axial mean velocity in the proximity of the free surface (Fig. 6a, Fig. 7a), and overestimated the turbulent velocities outside the plume region (Fig. 8a). This is due to a phenomenon of increased turbulence kinetic energy dissipation in the region of the free surface, which is not captured by the stan-

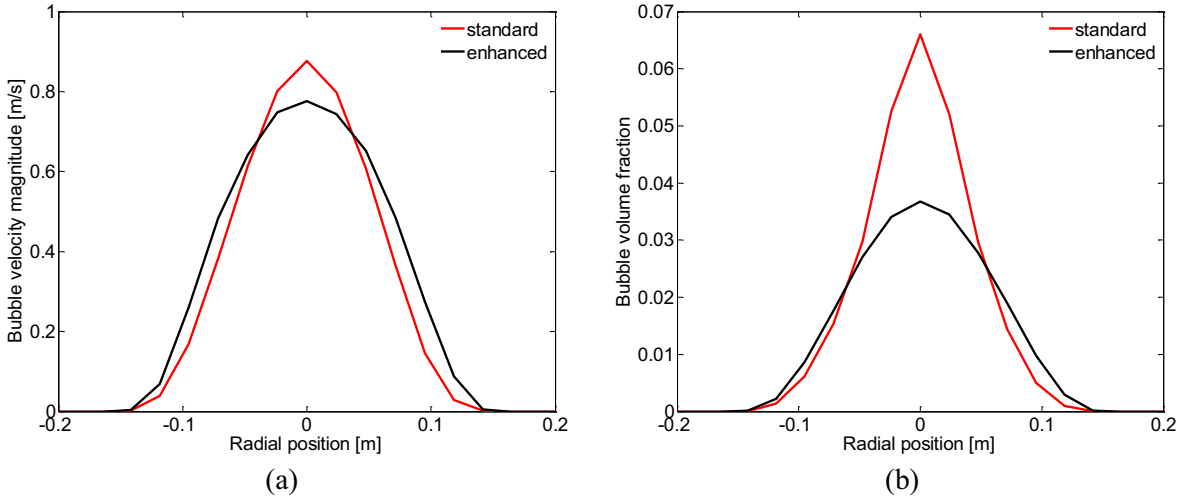

Fig. 5. Simulated profiles of bubble velocity magnitude (a) and bubble volume fraction (b) along radial position at 0.625 m height in the standard (red curve) and enhanced turbulence model (black curve) implementations, respectively, with flowrate of 4.7×10^{-4} m^3/s. (For interpretation of the references to colour in this figure legend, the reader is referred to the web version of this article.)

dard model. When turbulent eddies approach and locally lift a free surface, the turbulence is damped by the stagnation pressure (Cloete et al., 2009; Johansen and Boysan, 1988). The turbulence model implemented with free surface damping effects (blue dotted lines) was intended to provide a reasonable turbulence length scale, by which the velocity profiles can be improved compared with the standard model (Fig. 6a, Fig. 7a). Combining Fig. 6a and Fig. 6b, it is seen that the proposed free surface damping model also reproduces the sharp increase of the radial velocity from 1.117 m height (0.02 m under the initial surface) to 1.222 m height (0.015 m under the initial surface). Thus, close to the surface, the enhanced implementation with surface damping effects has better consistency with the experimental data than the standard model. Further down in the water, there is less discrepancy between the models. This is as expected since the surface damping effects are likely to influence the surface region. This module has also proven to be promising at larger depths with larger flowrates (Olsen and Skjetne, 2016).

The buoyancy-modified turbulence model was intended to account for the non-uniform distribution of bubbles: there is added turbulence intensity in unstable stratified flow region and suppressed turbulence in stable stratified flows. Compared with the standard model, the implementation with buoyancy-modified effects (green dotted lines) tend to produce a much wider and milder plume than the reality: decreased axial velocity near the centre of the plume and increased axial velocity away from the plume centre (Fig. 7); correspondingly, the simulated profiles of turbulence velocities and the bubble distributions also exhibit a wider and milder behaviour (Fig. 8, Fig. 9). This tend to produce a more uniformly distributed plume, leading to more deviation from the experimental observation. This implies that buoyancy-modified turbulence only is not sufficient to account for the turbulence modification due to the bubble–liquid interactions.

The turbulence agitation effects due to the bubble wake are therefore implemented (magenta dotted lines). The enhanced implementation produced reduced upwelling velocity (Fig. 7) and

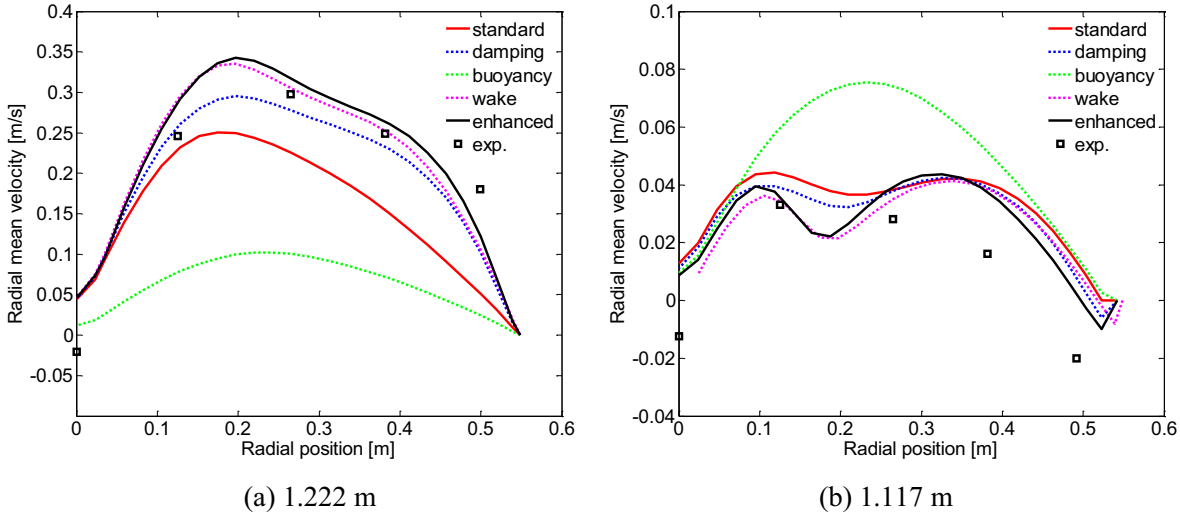

Fig. 6. Comparisons between simulated radial mean velocity and experimental data (□) along radial position at 1.222 m height (a) and 1.117 m height (b) with flowrate of 4.7×10^{-4} m^3/s. Simulations results with the standard k-epsilon model ('standard'), free surface damping module ('damping'), buoyancy-modified turbulence module ('buoyancy') and bubble-wake induced turbulence module ('wake'), and a complete version of the enhanced model ('enhanced') including the above three modules are shown by red solid lines, blue dotted lines, green dotted lines, magenta dotted lines and black solid lines, respectively. (For interpretation of the references to colour in this figure legend, the reader is referred to the web version of this article.)

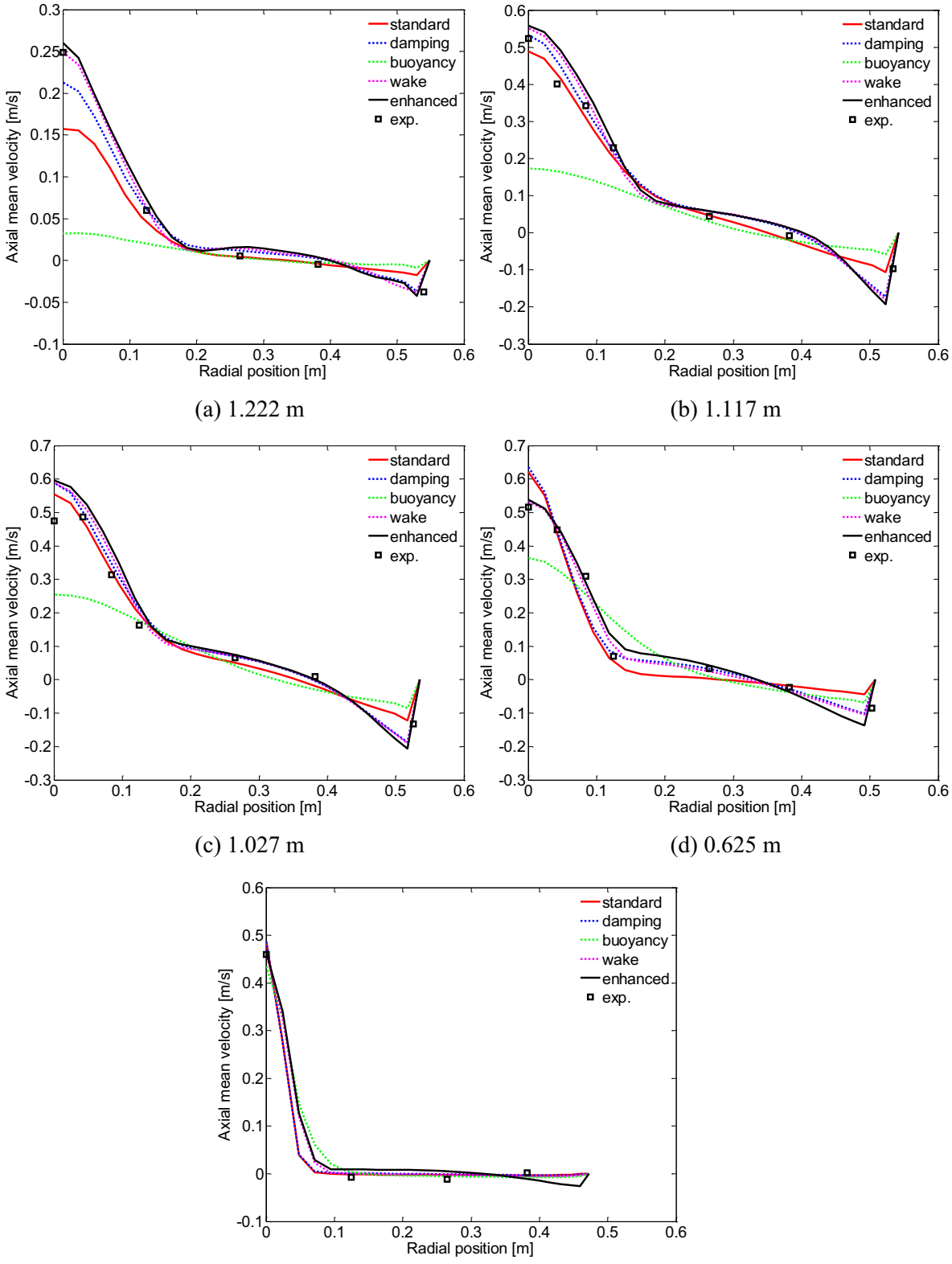

Fig. 7. Comparisons between simulated axial mean velocity and experimental data (□) along radial position at 1.222 m height (a), 1.117 m height (b), 1.027 m height (c), 0.625 m height (d), and 0.113 m height (e). See caption for Fig. 6.

enhanced turbulent velocity arising from the extra agitation (Fig. 8) in the plume centre regions, which are better consistency with the experiment. This modification of the turbulent kinetic energy created by the bubbles results from an equilibrium between the production and dissipation due to their presence (Lance and Bataille, 1991). Correspondingly, the bubbles give rise

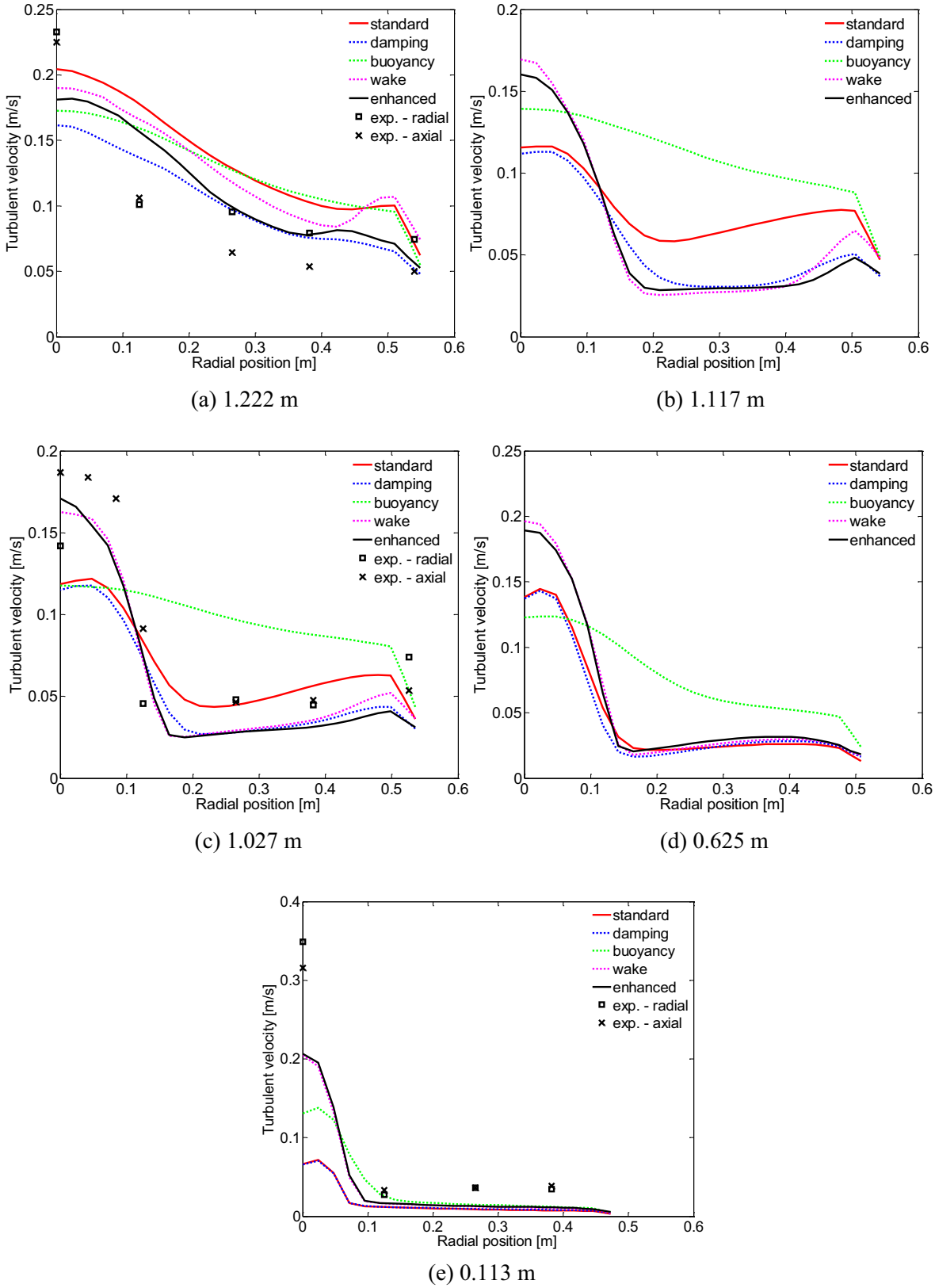

Fig. 8. Comparisons between simulated turbulent velocity and experimental data (radial direction: □; axial direction: ×) along radial position at 1.222 m height (a), 1.117 m height (b), 1.027 m height (c), 0.625 m height (d), and 0.113 m height (e). See caption for Fig. 6.

to a wider plume since they are susceptible to stronger turbulence fluctuations (Fig. 9), which improved the overestimated volume fractions with the standard model. The radial velocities at the interface are also improved (Fig. 6).

The complete version of the enhanced model (black solid lines) accounting for the free surface damping, buoyancy-modified turbulence and bubble wake was implemented. In the upwelling plume region, the standard model produced a narrower plume

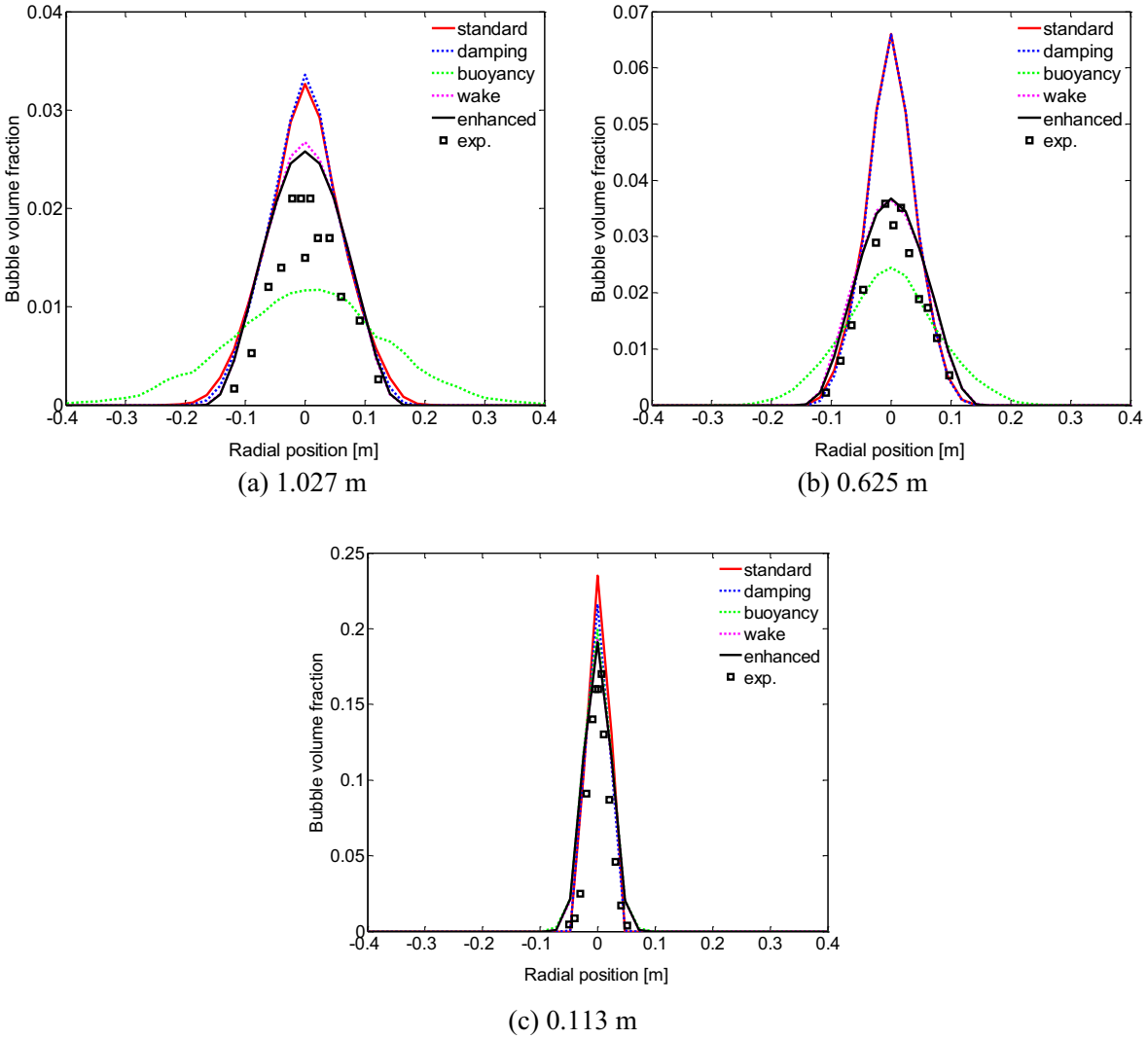

Fig. 9. Comparisons between simulated volume fraction and experimental data (□) along radial position at 1.027 m height (a), 0.625 m height (b), and 0.113 m height (c). See caption for Fig. 6.

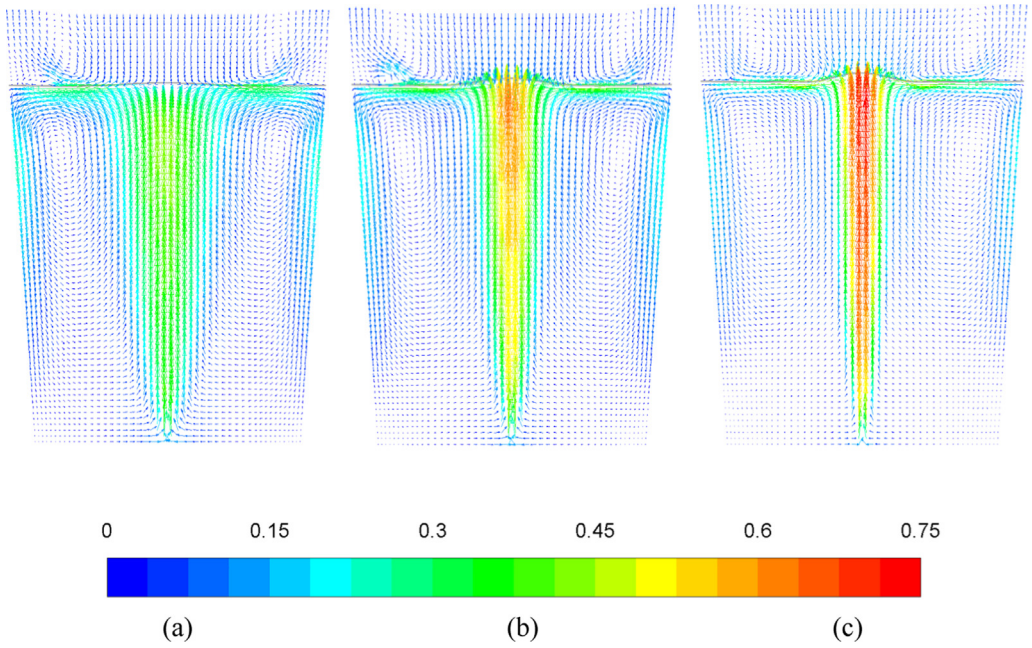

Fig. 10. Simulated velocity vector coloured by velocity magnitude with different model parameters 0.01 (a), 0.02 (b), 0.03 (c) with flowrate of 4.7×10^{-4} m^3/s. The location of the free surface is indicated by grey curves.

(Fig. 4c) than the reality, resulting in overestimation of upwelling velocity and bubble volume fraction (Fig. 7c-e and Fig. 9c-e). The deviations from the experiment can be 20% larger in upwelling velocity (Fig. 7d) and 95% larger in bubble volume fraction at the plume centre half way up (Fig. 9d). The standard model also underestimated the turbulent velocity in these bubble populated regions (Fig. 8c-e). Compared with the experiment, the enhanced implementation obviously improved the model performance in the upwelling plume region. In the vicinity of the surface, the standard model underestimates the axial velocity at the plume centre by 37% (Fig. 7a), and can underestimate the radial velocity by 36% (Fig. 6a). Compared with the experiment, the enhanced turbulence model developed show satisfactory quantitative agreement, which enables more accurate simulation in the transport at the surface region. It is noted that close to free surface, the radial turbulent velocity attains higher values than the axial (Fig. 8a). This is an effect of the geometrical restrictions of the free surface, which damps the axial velocity fluctuations. On the contrary, in the upwelling plume, axial fluctuation is dominant due to the presence of the gravity (Fig. 8c). However, this anisotropy cannot be resolved by k-epsilon models. A differential or algebraic Reynolds stress model could moreover account for this effect.

4.4. Significance of bubble-wake induced turbulence modelling

The algorithms for bubble-wake induced turbulence model are discussed in Section 3.3. The source term in the TKE transport equation is modelled as the product of the drag force and bubble–liquid relative velocity. The corresponding source term in turbulent dissipation transport equation rely on proper modelling of the pseudo turbulence time scale τ_{wake} and the model coefficient C^{ε}_{wake}. The former is independent on the pseudo turbulence intensity δ. So, the modelling practice comes down to the parameter choice of product of δ with C^{ε}_{wake}, which are not known a priori. The product of δ and C^{ε}_{wake} is tuned to be 0.02, based on the experimental data for flowrate of 4.7×10^{-4} m^3/s from Johansen et al. (1988) and Elgsæter (1986). As indicated in Fig. 10, the implementation of different parameters (0.01,0.02,0.03) turned out to govern the extent of the plume dispersion. That is because the turbulence is driving the dispersion of the plume. With a underestimated model parameter, that is larger τ_{wake} (smaller δ) or smaller C^{ε}_{wake}, the turbulent dissipation rate is underestimated, which would produce a overestimated TKE, resulting in overestimated plume dispersion arising from the effects of agitated turbulence due to bubble wake. Correspondingly, the more wake entrainment, the

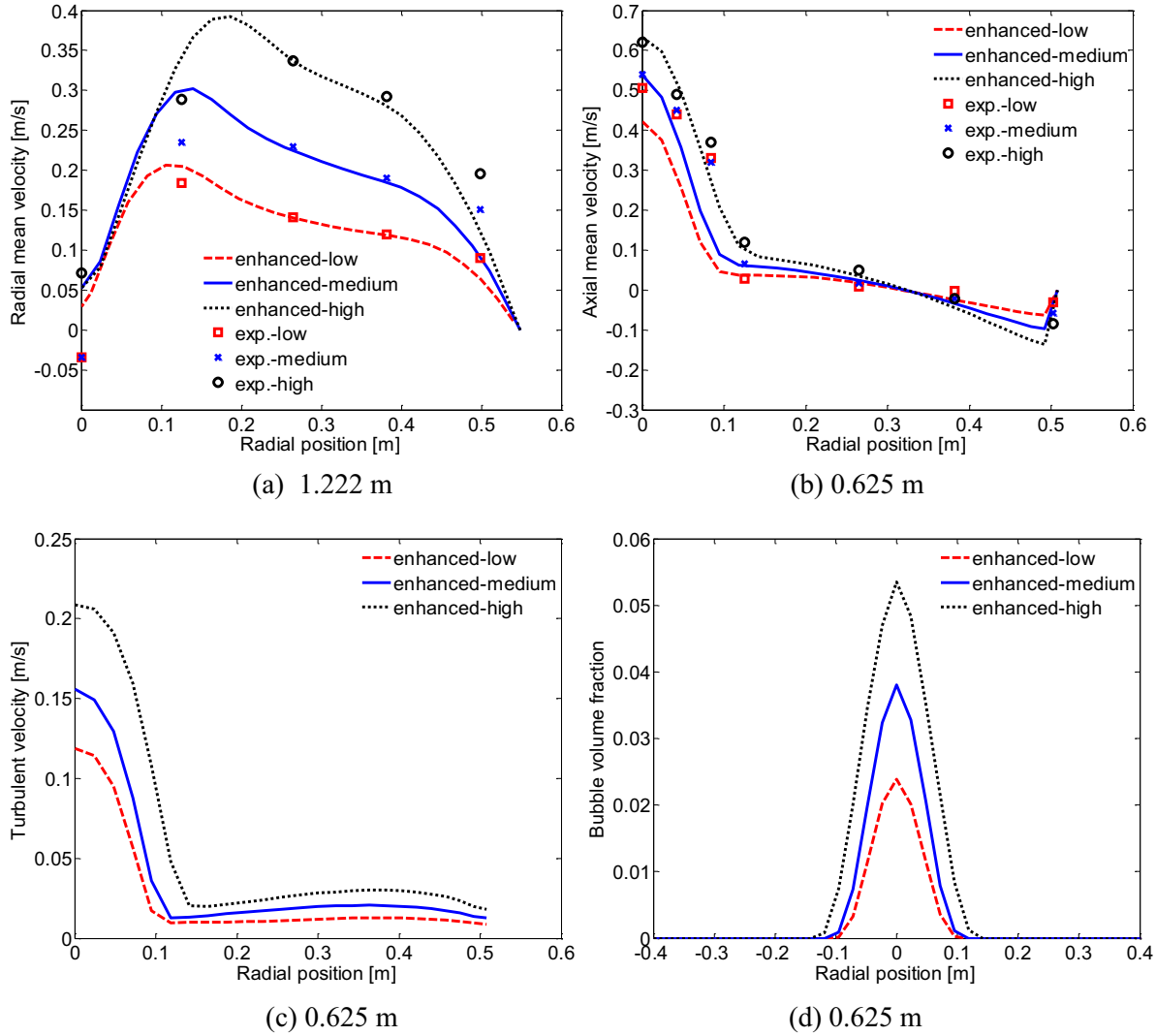

Fig. 11. Validations of the enhanced turbulent model against the experimental data for low 1.3×10^{-4} m^3/s (□), medium 2.7×10^{-4} m^3/s (×), and high flowrate 6.1×10^{-4} m^3/s (o) in terms of radial mean velocity (a), axial mean velocity (b), turbulent velocity (c) and bubble volume fraction (d). Simulations results with the low, medium and high flowrates are shown by red dashed lines, blue solid lines and black dotted lines, respectively. (For interpretation of the references to colour in this figure legend, the reader is referred to the web version of this article.)

more hindered momentum transfer from the bubbles to the water, which would result in a less upwelling plume.

The parameter in the bubble-wake model in this study is tuned and supported by the experiment. More physical formulation of pseudo-turbulence time scale and the coefficient for the source term in the turbulent dissipation equation should be further pursued, in order to predict the accurate extent of the plume dispersion.

4.5. Validations of the enhanced turbulence model

In order to perform the validation study, the proposed enhanced turbulence model was run with low 1.3 $\times$ 10^{-4} m^3/s, medium 2.7 $\times$ 10^{-4} m^3/s, and high flowrate 6.1 $\times$ 10^{-4} m^3/s in the experiment of Johansen et al. (1988). The comparisons of the radial velocity at the surface (1.222 m height) and axial velocity at half-way up the plume (0.625 m height), which are the representative features of the plume, are shown in Fig. 11. The simulated radial mean velocities are well validated against the experimental observations, and there exhibit distinct increase in the magnitude with the increase of the flowrate (Fig. 11a). The simulated radial mean velocities are also consistent with the observations, except that there is underestimation in the plume centre region for the low flowrate (Fig. 11b). Thus, it can be concluded that the proposed model is capable to reproduce the physics of the plume. With more air injecting into the ladle, both axial mean velocity and turbulent velocity (Fig. 11 c) are enhanced. Also, the plumes are populated with more bubbles, with the volume fraction increasing from ~ 2% to ~ 5% in the centre, and exhibit a wider trend. It is the larger turbulent velocity of the liquid phase, thus more turbulent dispersion, contributes to the wider plume. The conclusions are consistent with the findings of Lance and Bataille, (1991): the turbulent kinetic energy increases with the bubble volume fraction; when the bubble volume fraction exceed 1%, the hydrodynamic interactions between the bubbles contribute to the amplifying liquid turbulence.

5. Conclusions

An enhanced turbulence model which is an extension to the standard k-epsilon model has been developed and validated to make it more generally applicable to bubble plumes. Besides the bubble–liquid coupling in momentum, there is also the turbulence coupling. The effects of flow turbulence on bubbles are reflected by the turbulent dispersion force. The extra turbulence induced by bubbles through wake effects is accounted for by a proposed bubble-wake model. In addition, turbulence modulation due to bubble-induced stratification and added turbulent dissipation in the proximity of the free surface have been introduced. The enhanced turbulence model was applied to a gas-stirred ladle experiment. The model framework is an Eulerian-Lagrangian large scale interface-capturing CFD approach, coupling discreate phase model with volume-of-fluid model.

A series of dependency studies and analysis of the integral property ensured the proper implementation of the models. The implications of each physical process in turbulence modelling are investigated. The detailed comparison with experimental data, in terms of mean flow, turbulence and bubble distribution, indicate that the enhanced turbulence model allows improved representation of the physics of bubble plumes, as well as the transport phenomena at, and close to, the free surface. It was found that in the bubble wake model, the pseudo turbulence time scale and the coefficient in the turbulent dissipation transport equation appears to be crucial in obtaining the accurate extent of plume dispersion, which would require additional physical modelling studies.

CRediT authorship contribution statement

Qingqing Pan: Conceptualization, Methodology, Software, Formal analysis, Validation, Writing - original draft. **Stein Tore Johansen:** Conceptualization, Methodology, Supervision, Investigation, Writing - review & editing. **Jan Erik Olsen:** Methodology, Supervision, Project administration. **Mark Reed:** Conceptualization, Supervision, Writing - review & editing, Funding acquisition. **Lars Roar Sætran:** Supervision, Resources.

Declaration of Competing Interest

The authors declare that they have no known competing financial interests or personal relationships that could have appeared to influence the work reported in this paper.

Acknowledgments

This work was supported by the Research Council of Norway (Norges Forskningsråd) through project of oil spill containment by use of air bubbles 187376/S30, as well as the SURE project supported by Gassco, Statoil, BP, Shell, Total, Safetec, Wild Well Control, DNVGL, Petroleum Safety Authority Norway and SINTEF. Dr. Schalk Cloete from SINTEF, Dr. Lihao Zhao and Dr. Tian Li from NTNU, and Dr. Lei Wang from Sun Yat-sen University are also acknowledged for helpful discussions.

References

Besbes, S., El Hajem, M., Aissia, H.B., Champagne, J.-Y., Jay, J., 2015. PIV measurements and Eulerian-Lagrangian simulations of the unsteady gas–liquid flow in a needle sparger rectangular bubble column. Chem. Eng. Sci. 126, 560–572.

Buwa, V.V., Deo, D.S., Ranade, V.V., 2006. Eulerian-Lagrangian simulations of unsteady gas–liquid flows in bubble columns. Int. J. Multiph. Flow 32, 864–885.

Cloete, S., Olsen, J.E., Skjetne, P., 2009. CFD modeling of plume and free surface behavior resulting from a sub-sea gas release. Appl. Ocean Res. 31, 220–225.

Daly, B.J., Harlow, F.H., 1970. Transport equations in turbulence. Phys. Fluids 13, 2634–2649.

Dhotre, M.T., Smith, B.L., 2007. CFD simulation of large-scale bubble plumes: Comparisons against experiments. Chem. Eng. Sci. 62, 6615–6630.

Elgsæter, A., 1986. Bubble dynamics in the injection of gas in liquid (Bobledynamikk ved injeksjon av gass i væske). Norwegian University Science of Technology, Trondheim.

Fanneløp, T., Sjøen, K., 1980. Hydrodynamics of Underwater Blowouts, in: 18th Aerospace Sciences Meeting, Aerospace Sciences Meetings. American Institute of Aeronautics and Astronautics. https://doi.org/10.2514/6.1980-219

Feng, Q., Ge, R., Sun, Y., Fang, F., Luo, J., Xue, Z., Cao, J., Li, M., 2020. Revealing hydrodynamic effects on flocculation performance and surface properties of sludge by comparing aeration and stirring systems via computational fluid dynamics aided calculation. Water Res. 115500.

Feng, Y., Schwarz, M.P., Yang, W., Cooksey, M., 2015. Two-phase CFD model of the bubble-driven flow in the molten electrolyte layer of a Hall-Héroult aluminum cell. Metall. Mater. Trans. B 46, 1959–1981.

Fleck, S., Rzehak, R., 2019. Investigation of bubble plume oscillations by Euler-Euler simulation. Chem. Eng. Sci. 207, 853–861.

Fraga, B., Stoesser, T., Lai, C.C.K., Socolofsky, S.A., 2016. A LES-based Eulerian-Lagrangian approach to predict the dynamics of bubble plumes. Ocean Model. 97, 27–36.

Gosman, A., Loannides, E., 1983. Aspects of computer simulation of liquid-fueled combustors. J. Energy 7, 482–490.

Henkes, R., Van Der Vlugt, F., Hoogendoorn, C., 1991. Natural-convection flow in a square cavity calculated with low-Reynolds-number turbulence models. Int. J. Heat Mass Transf. 34, 377–388.

Huda, K.N.U., Shimizu, K., Gong, X., Takagi, S., 2018. Numerical investigation of COD reduction in compact bioreactor with bubble plumes. Chem. Eng. Sci. 185, 1–17.

Imteaz, M.A., Asaeda, T., 2000. Artificial mixing of lake water by bubble plume and effects of bubbling operations on algal bloom. Water Res. 34, 1919–1929.

Ishii, M., 1975. Thermo-fluid dynamic theory of two-phase flow. NASA Sti/recon Technical Report A 75.

Johansen, Ø., 2000. DeepBlow – a Lagrangian plume model for deep water blowouts. Spill Sci. Technol. Bull. 6, 103–111.

Johansen, S., Boysan, F., 1988. Fluid dynamics in bubble stirred ladles: Part II. Mathematical modeling. Metall. Trans. B 19, 755–764.

Johansen, S.T., 1990. On the Modelling of Disperse Two-phase Flows. Norwegian University Science of Technology, Trondheim.

Johansen, S.T., Robertson, D., Woje, K., Engh, T.A., 1988. Fluid dynamics in bubble stirred ladles: Part I. Experiments. Metall. Trans. B 19, 745–754.
Kataoka, I., 1986. Local instant formulation of two-phase flow. Int. J. Multiph. Flow 12, 745–758.
Lance, M., Bataille, J., 1991. Turbulence in the liquid phase of a uniform bubbly air–water flow. J. Fluid Mech. 222, 95–118.
Launder, B.E., Spalding, D.B., 1983. The numerical computation of turbulent flows, in: Numerical Prediction of Flow, Heat Transfer, Turbulence and Combustion. Elsevier, pp. 96–116.
Lee, J.H., Cheung, V., 1990. Generalized Lagrangian model for buoyant jets in current. J. Environ. Eng. 116, 1085–1106.
Lopez de Bertodano, M., Lahey Jr, R., Jones, O., 1994. Development of a k-ε model for bubbly two-phase flow.
Masterov, M.V., Baltussen, M.W., Kuipers, J.A.M., 2018. Numerical simulation of a square bubble column using Detached Eddy Simulation and Euler-Lagrange approach. Int. J. Multiph. Flow 107, 275–288.
McClimans, T., Leifer, I., Gjøsund, S.H., Grimaldo, E., Daling, P., Leirvik, F., 2013. Pneumatic oil barriers: The promise of area bubble plumes. Proc. Inst. Mech. Engineers, Part M: J. Eng. Maritime Environ. 227, 22–38.
Milgram, J., 1983. Mean flow in round bubble plumes. J. Fluid Mech. 133, 345–376.
Naot, D., Rodi, W., 1983. Interactions of turbulent eddies with a free surface. Prog. Astro. Aero. 84, 98–112.
Olsen, J.E., Popescu, M., 2012. On the effect of lift forces in bubble plumes. Presented at the proceedings of Ninth International Conference on CFD in the Minerals and Process Industries.
Olsen, J.E., Skjetne, P., 2020. Summarizing an Eulerian-Lagrangian model for subsea gas release and comparing release of CO2 with CH4. Appl. Math. Model. 79, 672–684.
Olsen, J.E., Skjetne, P., 2016. Modelling of underwater bubble plumes and gas dissolution with an Eulerian-Lagrangian CFD model. Appl. Ocean Res. 59, 193–200.
Pan, Q., 2014. Modelling of turbulent flows with strong dispersed phase-continuous fluid interactions. Norwegian University Science of Technology, Trondheim.
Pan, Q., Johansen, S.T., Cloete, S., Reed, M., Sætran, L., 2013. An enhanced k-epsilon model for bubble plumes. Presented at the Proceedings of the Eighth International Conference on Multiphase Flow.
Risso, F., 2018. Agitation, mixing, and transfers induced by bubbles. Annu. Rev. Fluid Mech. 50, 25–48.
Rzehak, R., Krepper, E., 2013. Bubble-induced turbulence: Comparison of CFD models. Nucl. Eng. Des. 258, 57–65.
Sánchez, F., Rey, H., Viedma, A., Nicolás-Pérez, F., Kaiser, A., Martínez, M., 2018. CFD simulation of fluid dynamic and biokinetic processes within activated sludge reactors under intermittent aeration regime. Water Res. 139, 47–57.
Sato, Y., Sekoguchi, K., 1975. Liquid velocity distribution in two-phase bubble flow. Int. J. Multiph. Flow 2, 79–95.
Sheng, Y., Irons, G., 1993. Measurement and modeling of turbulence in the gas/liquid two-phase zone during gas injection. Metall. Trans. B 24, 695–705.
Soga, C.L., Rehmann, C.R., 2004. Dissipation of turbulent kinetic energy near a bubble plume. J. Hydraul. Eng. 130, 441–449.
Sun, Y., Cao, X., Liang, F., Bian, J., 2020. Investigation on underwater gas leakage and dispersion behaviors based on coupled Eulerian-Lagrangian CFD model. Process Saf. Environ. Prot. 136, 268–279.
Tomiyama, A., 1998. Struggle with computational bubble dynamics. Multiphase Sci. Technol. 10, 369–405.
Troshko, A., Hassan, Y., 2001. A two-equation turbulence model of turbulent bubbly flows. Int. J. Multiph. Flow 27, 1965–2000.
Vaidheeswaran, A., Hibiki, T., 2017. Bubble-induced turbulence modeling for vertical bubbly flows. Int. J. Heat Mass Transf. 115, 741–752.
Van Wijngaarden, L., 1998. On pseudo turbulence. Theor. Comput. Fluid Dyn. 10, 449–458.
Wu, K., Cunningham, S., Sivandran, S., Green, J., 2017. Modelling subsea gas releases and resulting gas plumes using computational fluid dynamics. J. Loss Prev. Process Ind. 49, 411–417.
Xia, L., Law, A.-W.-K., Fane, A.G., 2013. Hydrodynamic effects of air sparging on hollow fiber membranes in a bubble column reactor. Water Res. 47, 3762–3772.
Youngs, D.L., 1982. Time-dependent multi-material flow with large fluid distortion. Numerical methods for fluid dynamics.
Yum, K., Kim, S.H., Park, H., 2008. Effects of plume spacing and flowrate on destratification efficiency of air diffusers. Water Res. 42, 3249–3262.
Zhang, K., Song, H., Wang, H., Tao, J., Guan, Y., Gong, Y., Fan, W., Geng, M., 2020. A preliminary study on the active cold seeps flow field in the Qiongdongnan Sea Area, the northern South China Sea. Chin. Sci. Bull. 65, 1130–1140.
Ziegenhein, T., Rzehak, R., Lucas, D., 2015. Transient simulation for large scale flow in bubble columns. Chem. Eng. Sci. 122, 1–13.